JOURNAL OF GEOPHYSICAL RESEARCH, VOL. 105, NO. B4, PAGES 7857–7871, APRIL 10, 2000

On rate-state and Coulomb failure models

J. Gomberg

U.S. Geological Survey, Center for Earthquake Research and Information, University of Memphis
Memphis, Tennessee

N. Beeler and M. Blanpied

U.S. Geological Survey, Menlo Park, California

Abstract. We examine the predictions of Coulomb failure stress and rate-state frictional models. We study the change in failure time (clock advance) Δt due to stress step perturbations (i.e., coseismic static stress increases) added to "background" stressing at a constant rate (i.e., tectonic loading) at time t_0. The predictability of Δt implies a predictable change in seismicity rate $r(t)/r_0$, testable using earthquake catalogs, where r_0 is the constant rate resulting from tectonic stressing. Models of $r(t)/r_0$, consistent with general properties of aftershock sequences, must predict an Omori law seismicity decay rate, a sequence duration that is less than a few percent of the mainshock cycle time and a return directly to the background rate. A Coulomb model requires that a fault remains locked during loading, that failure occur instantaneously, and that Δt is independent of t_0. These characteristics imply an instantaneous infinite seismicity rate increase of zero duration. Numerical calculations of $r(t)/r_0$ for different state evolution laws show that aftershocks occur on faults extremely close to failure at the mainshock origin time, that these faults must be "Coulomb-like," and that the slip evolution law can be precluded. Real aftershock population characteristics also may constrain rate-state constitutive parameters; a may be lower than laboratory values, the stiffness may be high, and/or normal stress may be lower than lithostatic. We also compare Coulomb and rate-state models theoretically. Rate-state model fault behavior becomes more Coulomb-like as constitutive parameter a decreases relative to parameter b. This is because the slip initially decelerates, representing an initial healing of fault contacts. The deceleration is more pronounced for smaller a, more closely simulating a locked fault. Even when the rate-state Δt has Coulomb characteristics, its magnitude may differ by some constant dependent on b. In this case, a rate-state model behaves like a modified Coulomb failure model in which the failure stress threshold is lowered due to weakening, increasing the clock advance. The deviation from a non-Coulomb response also depends on the loading rate, elastic stiffness, initial conditions, and assumptions about how state evolves.

1. Introduction

The apparent ability of stress changes that are orders of magnitude smaller than earthquake stress drops to alter seismicity rates or to promote or inhibit moderate or large earthquakes can be explained if the influenced faults are highly prestressed and the stress changes advance or retard their failure times. Both Coulomb failure stress and rate-state frictional models have been used to predict these "clock advances" (or "clock delays") [*Harris and Simpson*, 1992, 1998; *King et al*., 1994; *Hardebeck et al*., 1998; *Nalbant et al*., 1998; *Nostro et al*., 1998; *Dieterich*, 1992, 1994]. Clock advance or delay Δt refers to the change in failure time, which is most often attributed to coseismic (static) stress changes. We examine theoretically the different predictions of these two models and the parameters that most affect them. We demonstrate that a rich variety of clock advance predictions are possible, depending on the fault, on material and loading properties, and on the constitutive laws invoked. We also show that the clock advances predicted by rate-state models asymptotically become equivalent to Coulomb clock advances under a variety of conditions.

This variety of predicted responses to stress perturbations suggests that field and laboratory measurements may allow us to identify particular constitutive and failure relations as more appropriate than others. *Blanpied et al*. [1999] discuss results of laboratory experiments in which the effect of stress history on the timing and peak stress of stick-slip events were studied in the context of various constitutive and failure relations. Although measurement of clock advance for single earthquakes in the Earth is difficult, seismicity rate changes offer the potential to test predictions of Δt and thus to discriminate among failure models and their controlling parameters. As discussed by N. M. Beeler et al. (manuscript in preparation, 2000), observations of aftershock sequences require a time-dependent failure process. This process may be characterized in terms of a time-dependent Δt, for example, as predicted by some rate-state models. *Dieterich* [1992, 1994] noted this and derived analytic approximate formulas describing the change in seismicity rate following a mainshock for a specific frictional law [*Harris and Simpson*, 1998; *Toda et al*., 1998; *Belardinelli et al*., 1999]. We take a more general approach and numerically compute changes in seismicity rates for a variety of constitutive

Paper number 1999JB900438.

laws and model parameters and compare them to characteristics of real aftershock sequences.

We first summarize the basic ideas underlying Coulomb and rate-state failure models. We then derive general formulas for seismicity rate changes caused by stress perturbations and apply these to look at the effect of tectonic stressing and coseismic stress changes expected in real earthquake sequences, assuming Coulomb or rate-state failure models apply. We conclude with a simple theoretical analysis and illustrative examples (assuming parameters appropriate to laboratory conditions) that demonstrate how and why the timing of failure predicted by the Coulomb and rate-state models differ and under what conditions they become nearly identical.

2. Failure Models

We begin by summarizing the basic ideas underlying Coulomb and rate-state failure models.

2.1. Coulomb Failure Model

The notion of a clock advance (or delay) is most easily understood in the context of a Coulomb failure stress (CFS) model (see *Harris* [1998] for a summary). The failure criterion simply requires reaching a critical stress threshold equal to $\tau + \mu(\sigma_n + P) - S$, in which τ is the shear traction, σ_n is normal traction, and P is the pore pressure. The coefficient of friction μ and the cohesion S are both assumed to be constant. Positive changes in the tractions and/or pore pressure move a fault closer to the failure stress by an amount $\Delta\text{CFS} = \Delta\tau + \mu(\Delta\sigma_n + \Delta P)$. This corresponds to a clock advance of $\Delta t_{\text{Coulomb}} = \Delta\text{CFS}/(d\tau_b/dt)$, in which $d\tau_b/dt$ is the background Coulomb stressing rate. The clock advance is independent of when the ΔCFS occurs, and no slip occurs during loading. These characteristics and the linear relationship between stress change and Δt are not implicit in rate-state frictional models.

2.2. Rate-State Model

Unlike Coulomb failure, rate-state failure does not invoke a threshold stress. Instead, the failure criterion suggested by *Dieterich* [1986, 1992, 1994] requires the slip velocity to reach some high value. This definition is particularly appropriate for rate-state failure where slip velocity gradually increases prior to dynamic slip. We define earthquake recurrence or cycle time as the duration required for the slip velocity to evolve from some initial value at or below the background rate, representing the velocity immediately following a previous failure, to some very high value at which the acceleration becomes large enough to represent earthquake failure. The slip evolution is governed by the frictional rate-state constitutive relation [*Dieterich*, 1979; *Ruina*, 1983], describing the frictional strength $\tau(t)$ of a fault as

$$\tau(t) = \sigma_n\mu(t) = \sigma_n[\mu_0 + a \ln (V(t)/V_0) + b \ln (V_0\xi(t)/d_c)]. \quad (1)$$

The ξ has been interpreted as a measure of the connectivity of contacts on a fault surface or within a fault gouge. Connectivity might be related to the area of the contact which can increase with age [*Dieterich*, 1979] or could be related to porosity [*Sleep*, 1995]. The a, b, and d_c are empirical constants, V_0 and μ_0 are arbitrary reference values, and σ_n is the normal stress, assumed here to be constant.

We consider a simple single spring-slider system [*Dieterich*, 1981] in which the shear stress applied to the spring at the load point is governed by Hooke's law

$$\tau(t) = \sigma_n k[x_{lp}(t) - x(t)], \quad (2a)$$

in which x_{lp} is the load point displacement, x is the fault slip, and k is the stiffness. Thus the rate of change of shear stress is

$$d\tau(t)/dt = \sigma_n k[dx_{lp}(t)/dt - V(t)]. \quad (2b)$$

The system is loaded at constant background rate V_b with or without an additional perturbation of amplitude Δx_{lp} and time history described by a Heaviside or step function applied at time t_0 (i.e., $H(t - t_0)$) such that

$$dx_{lp}(t)/dt = V_b + \Delta x_{lp}\, dH(t - t_0)/dt = V_b + \Delta x_{lp}\delta(t - t_0). \quad (2c)$$

The final step to completely describing the system's behavior is to specify how $\xi(t)$ changes with time. To allow for a range of responses, we consider equations for the derivative of $\xi(t)$ for two state "evolution laws" (both are empirical relations); the first is the "slowness law"

$$d\xi/dt = 1 - V(t)\xi(t)/d_c, \quad (3a)$$

and the second is the "slip law" [*Ruina*, 1983].

$$d\xi/dt = -V(t)\xi(t)/d_c \ln [V(t)\xi(t)/d_c]. \quad (3b)$$

Physically, these "laws" have very different implications for how a fault surface evolves. Although a number of physical interpretations have been ascribed to ξ, all pertain to the connectivity of contacts on a fault surface. Thus we use the terms strengthening (increasing ξ) and weakening (decreasing ξ) to refer to changes in this connectivity that cause slip to be inhibited or facilitated, regardless of the specific mechanism. The slowness law implies strengthening ($d\xi/dt \sim 1$) when the fault is stationary or slipping sufficiently slowly and implies weakening ($d\xi/dt < 0$) only when slip is rapid. The slip law implies that a fault surface strengthens ($d\xi/dt > 0$) when the slip velocity satisfies $0 \ll V\xi/d_c < 1$ and weakens ($d\xi/dt < 0$) only at very high velocity when $V\xi/d_c > 1$. The fault surface essentially does not change when stationary or slowly slipping ($d\xi/dt \sim 0$ [see *Beeler et al*., 1994; *Nakatani*, 1998].

The unperturbed and perturbed cycle times t_b and t_p, respectively, and the clock advance $\Delta t = t_b - t_p$ are computed following the procedure described by *Gomberg et al*. [1997]. In short, the time derivatives of μ, x_{lp}, and ξ are calculated at each time step according to (2b), (2c), and (3), respectively. The μ, x_{lp}, and ξ are calculated at subsequent time steps using a Runga-Kutta algorithm, and V is found using (1). Failure occurs at the time when the calculations become numerically unstable and are stopped. Because the final acceleration is so rapid, the precise velocity at which instability occurs makes negligible difference to the total cycle times or clock advances. Initial values V_{init} and ξ_{init} and constants μ_0 and V_0 were chosen to be appropriate for the start of an earthquake cycle (after any postseismic slip from a previous event) and so that cycle times corresponded to those of large earthquakes (Figures 2–5) or laboratory experiments (Figures 6–9) [see *Gomberg et al*., 1997]. We leave study of the effect of variations in normal stress for subsequent studies and do not consider inertial effects. The latter is justified because we do not attempt to model the rupture process itself but only the evolu-

tion up to the point at which rupture becomes dynamic. Even if our model velocities reach values at which dynamic effects should become significant, again, they do so only when an insignificant fraction of the cycle is left so that the error should be insignificant.

3. Seismicity Rate Changes

We now derive formulas for seismicity rate changes caused by static stress perturbations. The formulas are general, applicable with any failure model and any type of stressing time history. We apply these in several illustrative examples using numerical calculations of the responses of spring-slider systems obeying rate-state frictional laws. We employ a constant rate "background" stressing rate with the addition of a positive step function stress change. This stressing history simulates that of tectonic stressing and coseismic stress changes, and model parameters are chosen to match those in real earthquake sequences. We compare the rate-state predictions for both the slip and slowness state evolution laws to the predictions of a Coulomb model and to the approximate formulation of *Dieterich* [1992, 1994].

Coulomb failure models cannot explain observations of delayed failure. This is most evident in aftershock sequences, which often follow Omori's empirical law [*Dieterich*, 1994; N. M. Beeler et al., manuscript in preparation, 2000] that describes the rate of earthquake occurrence $r(t)$ as a function of the time since the mainshock t as

$$r(t) = K/(c + t)^p. \tag{4}$$

K, c, and p are empirical constants [*Utsu et al*., 1995]. A dependence of clock advance on stressing history offers one possible explanation for the appropriateness of Omori's law. Although we do not attempt to match $r(t)$ for any particular aftershock sequence, our modeling shows that three of the characteristics common to nearly all aftershock sequences provide constraints on combinations of the constitutive parameters and probably cannot be fit with the slip state evolution law (equation (3b)). The characteristics we require viable models to predict include the following: (1) The decay rate is consistent with $p \sim 1$ in (4) [*Kisslinger and Hasegawa*, 1991; *Kisslinger and Jones*, 1991; *Dieterich*, 1994; *Utsu et al*., 1995]. (2) The seismicity rate returns from elevated rates directly to the constant background rate r_0 (i.e., $r(t)/r_0 \geq 1$ always). (3) The aftershock sequence duration t_a is defined as the time required to return to r_0. This duration is a small fraction of the unperturbed mainshock cycle time t_{cycle} or $t_a/t_{\text{cycle}} \sim 0.4\%$ to 20%, with most estimates being considerably less than 10% [*Dieterich*, 1994; *Toda et al*., 1998].

3.1. Derivation of Seismicity Rate Change Formulas

If aftershocks are simply earthquakes that have been clock advanced by a mainshock, then a very simple formula describes the change in seismicity rate following the mainshock. The derivation of this formula requires the assumption that aftershocks occur on a collection of faults uniformly distributed within their failure cycles so that when loaded at a constant rate, failure occurs at constant rate r_0. We refer to this collection of faults as an "aftershock" fault population (Figure 1a). The seismicity rate following a stress step perturbation applied at t_0 varies as

$$r(t) = r_0[1 - dt_p/dt], \tag{5a}$$

where t_p is the perturbed failure time. As above, t is the time from the mainshock, or $t = t_p - t_0$. As will be demonstrated below, (5a) is valid even for populations containing faults with a variety of cycle times or, equivalently, a range of magnitudes.

Our understanding of how the timing of failure depends on loading history comes from previous studies that have considered only a single fault rather than a system of faults. For a single fault we examined the dependence of clock advance on when the perturbing stress is applied or, mathematically, the dependence of Δt or t_p on t_0 [*Gomberg et al*., 1997, 1998]. We also can study a collection of faults and employ the same computational tools by considering an alternative view of the aftershock fault population affected by a stress perturbation. In this completely equivalent view, instead of varying where the faults are in their cycles and applying the stress perturbation at a single t_0, all the faults in the population are at the same point in their cycles and are perturbed by stress steps applied at different, uniformly distributed values of t_0. We refer to this as the "calculation" fault population (Figure 1b).

To calculate the seismicity rate change, we construct a curve of Δt or t_p versus t_0 by doing a series of numerical calculations (as performed by *Gomberg et al*. [1998]) using an identical set of model parameters with only t_0 varied. As demonstrated in Appendix A, the seismicity rate change can then be calculated using formulas equivalent to (5a). These are

$$\begin{aligned} r(t) &= r_0/[1 + d\Delta t/dt_0] \\ &= r_0/[1 - dt_p/dt_0]. \end{aligned} \tag{5b}$$

Recall that as in (5a), $t = t_p - t_0$. *Dieterich* [1994] derived a very specific form of (5) in which he assumed fault systems are governed by rate-state friction (equation (1)) with state evolving according to an approximate form of the slowness law (equation (3a)) valid only during the final, self-accelerating phase of a cycle when slip rapidly accelerates toward failure.

Figure 2 illustrates the relationship between these aftershock and calculation fault populations and (5). We show calculations for model parameters appropriate to the Earth (see below) and a step function stress perturbation, first viewed as a calculation fault population; Figure 2b shows the t_p versus t_0 curve, calculated numerically according to the recipe described in section 2.2, along with the failure lines predicted by a Coulomb model. The diagonal line in Figure 2b corresponding to instantaneous failure, $t_p = t_0$, is equivalent to the mainshock onset time when considering the aftershock population (Figure 1a). The delay from instantaneous failure is the time variable $t = t_0 - t_p$ that determines the seismicity rate change $r(t)/r_0$. In other words, the aftershock fault population simply corresponds to the calculation population with a rereferencing of the timescale. We replot the failure curve in terms of the logarithm of this delay time (Figure 2a) to emphasize the time range over which t_p, and thus $r(t)/r_0$, varies most significantly.

Note that a perturbation applied early in the cycle (small t_0) corresponds to a fault that is far from failure or hardly prestressed when the mainshock occurs. Similarly, a late perturbation corresponds to a fault that is close to failure when the mainshock occurs. The transformation from t_0 to t highlights the fact that the rate change (Figure 2c) is determined primarily by the faults that are close to failure and for which t_p differs only very slightly from instantaneous failure. In other words, this shows explicitly that aftershocks occur on the most highly prestressed faults. This explains why the complete numerical calculation and curves describing the approximate *Dieterich*

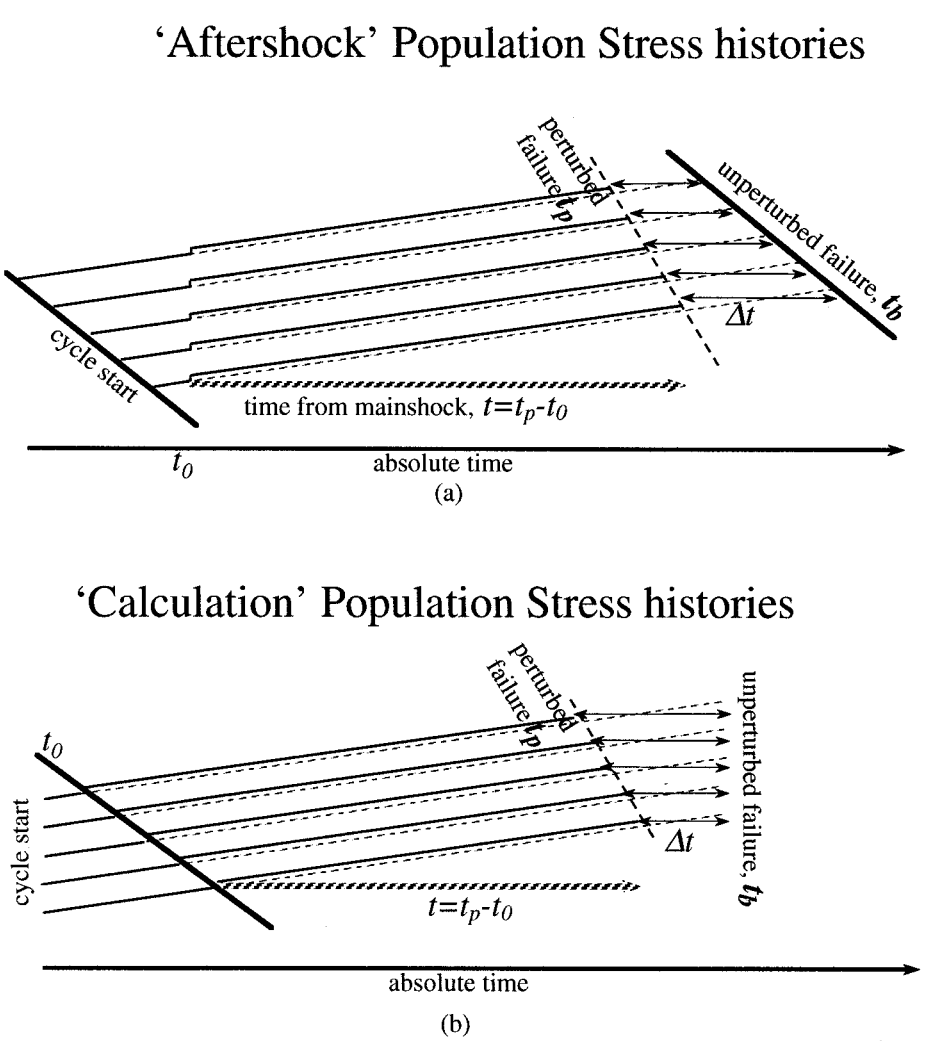

Figure 1. (a) Each diagonal line represents the stressing history of a fault that belongs to a population of faults that might correspond to those participating in an aftershock sequence. The stresses are distributed so that when stressed at a constant rate (dashed lines after t_0, solid lines before t_0), failure occurs at a constant rate r_0. Assuming all faults have equal unperturbed cycle durations, failure at r_0 corresponds to cycle start times distributed identically to the failure times t_b (indicated by thick diagonal lines, which all have equal slopes). The slope of the failure lines indicates the number of faults Δn that fail in a given time interval, that is, the seismicity rate dn/dt. If a stress step is added at time t_0 to the constant stressing (solid diagonal lines show the perturbed stress histories), the failure time of each fault will be advanced to t_p by clock advance Δt (double arrowhead lines). Because Δt depends on the stressing history prior to t_0, Δt may not be constant so that the failure rate changes and becomes a function of the time from t_0, $t = t_b - \Delta t - t_0 = t_p - t_0$. This new rate is $r(t)$. (b) Stressing histories of an equivalent distribution of faults to Figure 1a but more appropriate to what we actually calculate. In the absence of a perturbing stress, all faults have identical stressing histories, and a stress step perturbation is added at a different values of t_0, distributed identically to the failure times t_b in Figure 1a (thicker solid line has same slope). The clock advances are identical to those in Figure 1a. Thus the population in Figure 1a and $r(t)$ can be simulated by computing t_p for a single fault repeatedly but varying t_0 each time (see text). Note the arrow measuring t corresponds only to one fault or value of t_0.

[1994] equation for $r(t)/r_0$ agree so closely (Figure 2c); that is, it is because the *Dieterich* [1994] approximation is valid for faults already near failure. Significant differences in the clock advances predicted by the numerical calculations and the *Dieterich* [1994] formulation appear for small t_0 (Figure 2b), but this corresponds to faults that do not contribute to the aftershock sequence.

Finally, we consider the fact that real aftershock sequences contain earthquakes with a range of magnitudes and thus a range of cycle times. If the seismicity rate change is the same for all magnitudes (cycle times), then (5) may apply to sequences containing aftershocks of all sizes in any proportion. The above conclusion, that it is the faults already close to failure that compose the aftershock sequence, suggests that the cycle times of the aftershocks should not matter. In other words, it does not matter how long it took a fault to get close to failure, only that it is nearly ready to fail. Moreover, from Figure 2b it is apparent that a longer cycle time corresponds to shifting the failure curve upward along the instantaneous failure line, such that dt_p/dt and thus $r(t)/r_0$ change negligibly. We verified this by changing only the cycle times by altering the initial conditions and found that indeed $r(t)/r_0$ remained constant.

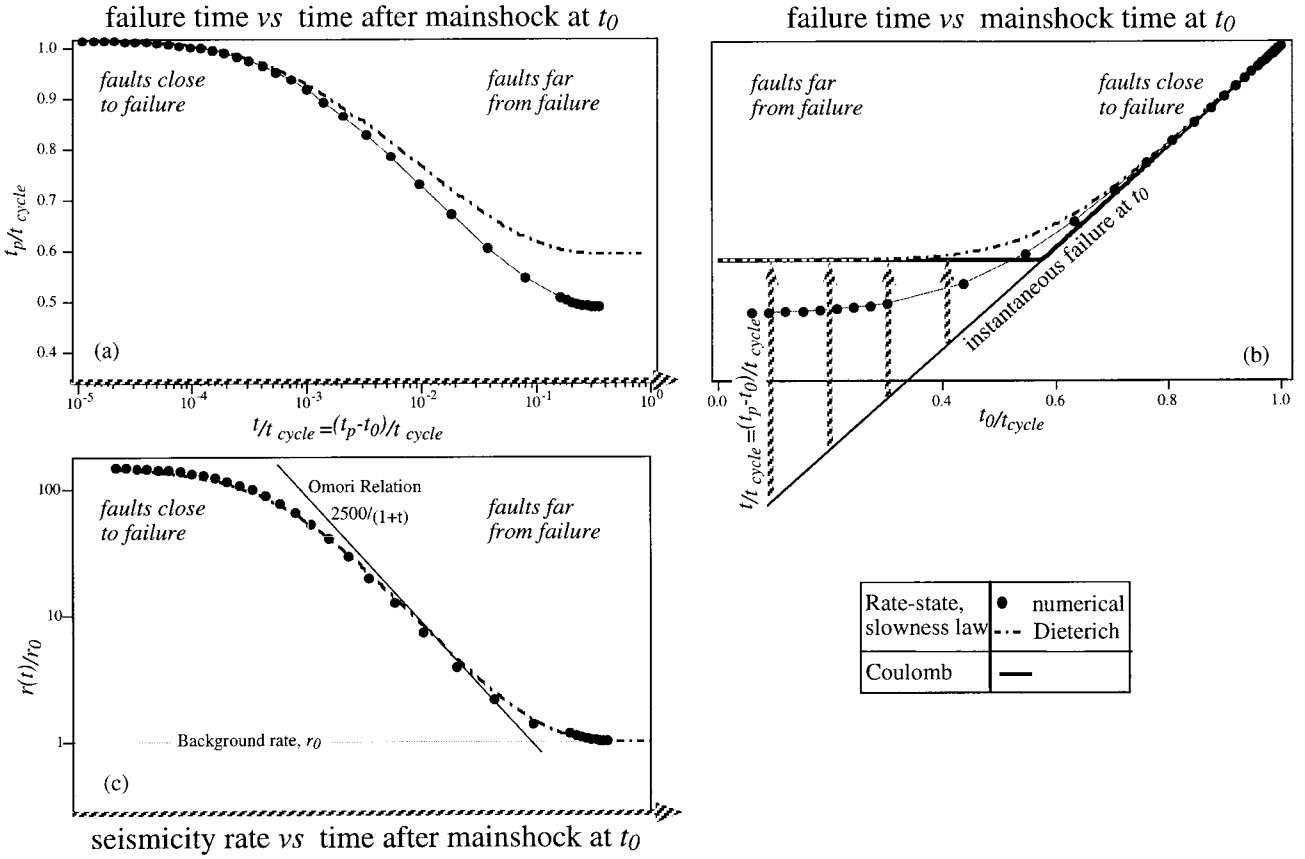

Figure 2. (a) Perturbed failure times t_p plotted as a function of t of a stress step for the model parameters in Table 1. Note the significant change in timescale compared to Figure 2b. (b) Same failure times plotted in Figure 2a but as a function of the onset time t_0. All times are normalized by the unperturbed cycle time, t_{cycle}. The t_p versus t_0 curves are shown for the complete rate-state solution calculated numerically (large dots connected by the light curve), predicted by a Coulomb model (thick straight lines), and calculated using the approximate formulation of *Dieterich* [1994] (dash-dotted curve). An early value of t_0 corresponds to perturbing a fault that is far from failure and a late t_0 to a fault that is close to failure. The line corresponding to instantaneous failure $t_p = t_0$ (thin diagonal line) is equivalent to the mainshock onset time. The delay from this (vertical striped arrows) is the time variable $t = t_0 - t_p$, corresponding to the time to failure from the mainshock and is the independent variable, or time axes, of the plots on the left (shown also by horizontal striped arrows). (c) The term $r(t)/r_0$ calculated numerically (large dots) according to (5) from the points defining the failure curve in Figure 2a. A hypothetical example of an aftershock rate following Omori's law (equation (4)) is shown (diagonal line); a closer fit at very short times can be obtained by increasing the constant added to t in the denominator, but such large values are not commonly observed.

3.2. Application to Real Aftershock Sequences

3.2.1. Parameter constraints. We study $r(t)/r_0$, which is calculated numerically, without *Dieterich*'s [1994] approximation for both the slip and slowness evolution laws to see if aftershock data distinguish between evolution laws and constitutive parameters. The $r(t)/r_0$ and failure curves are calculated numerically for two sets of model parameters and both the slip and slowness state evolution laws. The two models differ only in the assumed values of constitutive parameter a and step load amplitude Δx_{lp}. All parameters are chosen to be appropriate to real earthquakes or are from laboratory experiments when no other constraints exist (see Table 1). Laboratory experiments constrain constitutive parameters b and the larger value of a used [*Tse and Rice*, 1986; *Dieterich*, 1994; *Sleep*, 1995]. Parameter d_c ranges from 0.001 to 0.1 m on the basis of laboratory, field, and theoretical studies [*Roy and Marone*, 1996; *Tse and Rice*, 1986]. Step function perturbations are comparable to the coseismic slip in earthquakes with $M_w \sim 6$ ($\Delta x_{lp} = 0.1$ m and 0.0718 m for $a = 0.001$; Figure 5) and $M_w \sim 7$ ($\Delta x_{lp} = 1.0$ m and 0.819 m for $a = 0.01$; Figure 4) [*Wells and Coppersmith*, 1994]. We scale Δx_{lp} with a to correspond to the same approximate Omori decay (Figure 2) [*Dieterich*, 1994] and so that the Coulomb clock advances are the same fraction of the cycle time in models with $a = 0.01$ and $a = 0.001$. The background loading rate V_b approxi-

Table 1a. Fixed Parameters for Models in Figures 2, 4, and 5

Parameter	Value
b	0.015
μ_0	0.7
V_0, m/s	10^{-9}
d_c, m	0.01
V_{init}, m/s	10^{-9}

See text for justifications for this choice of parameters.

Table 1b. Varied Parameters for Models in Figures 2, 4, and 5

	State Evolution Law	a	k, m^{-1}	ξ_{init}, days	Δx_{lp}, m	Cycle Time, days
Figures 2 and 4	slowness	0.01	0.05	1.088 (10%)	1.0	27,232.4
	slip	0.01	0.05	1.088 (10%)	0.819	22,303.8
Figure 5	slowness	0.001	0.05	1.088 (10%)	0.1	35,259.3
	slip	0.001	0.05	1.088 (10%)	0.0718	25,323.6

Percentages specified next to ξ_{init} values indicate the corresponding initial value of μ relative to μ_0. See text for justifications for this choice of parameters.

mately equals that measured along the Pacific–North American plate margin in California. Initial values V_{init} and ξ_{init} and constants μ_0 and V_0 were chosen so that all numerical experiments resulted in comparable cycle times of the order of 100 years.

We summarize some of the observations that provide constraint on the stiffness, noting that most also require estimation of σ_n. *Walsh* [1971] defined $k\sigma_n$ as $G/w = \Delta\tau/\Delta x_{lp}$, in which w is the width of a fault that slipped Δx and G is the shear modulus. He estimated $k\sigma_n \sim 3$ MPa/m and noted that this exceeds laboratory values by 4 or 5 orders of magnitude. The ratio of slip to stress rate also provides a measure of k because the former equals V_b and the latter $d\tau_b/dt$ equals $k\sigma_n V_b$. From estimates made near the 1995 Kobe, Japan, earthquake, $k\sigma_n$ ranges from 0.4 to 4 MPa/m [*Toda et al*., 1998]. Corresponding estimates for faults near the 1989 Loma Prieta, California, earthquake are 0.8 to 5 MPa/m [*Gross and Burgmann*, 1998], and those from near the 1992 Landers, California, earthquake are 0.01 to 2 MPa/m [*Gross and Kisslinger*, 1997]. In their theoretical modeling, *Tse and Rice* [1986] assumed $k\sigma_n \sim 0.08$ MPa/m. *Roy and Marone* [1996] found even lower values of $k\sigma_n$, ~ 0.001 to 0.01 MPa/m, required to explain the apparent triggering threshold reported in other studies of triggering. If $\sigma_n \sim 100$ MPa, of the order of lithostatic stresses at seismogenic depths, then $k \sim 10^{-5}$ to 0.05 m^{-1}. We assume $k \sim 0.05$ m^{-1}.

3.2.2. Coulomb model seismicity rate change. Before discussing the rate-state results we first illustrate the generality of the model of aftershocks as clock advanced earthquakes on a special suite of faults and (5) by applying it to the Coulomb model. Figure 3 illustrates this schematically. Application of (5) shows that the model predicts an infinite rate change at the time of the mainshock and no change thereafter. Faults within $\Delta t_{\text{Coulomb}}$ of failure at the time of the mainshock fail instantaneously (Figure 3a); that is, $t_p = t_0$ and $dt_p/dt_0 = 1$ (Figure 3a, right), and thus $r(t)$ is infinite (equation (5b); Figure 3a, left). This infinite rate change occurs instantly at the time of the mainshock since $t = t_0 - t_p = 0$. All other faults are clock advanced identically by $\Delta t_{\text{Coulomb}}$, so that $dt_p/dt_0 = 0$ (Figure 3b, right), and there is no rate change (equation (5b); Figure 3b, left).

3.2.3. Rate-state, slip law model seismicity rate change. The $r(t)/r_0$ calculated assuming a slip state evolution law is inconsistent with aftershock sequence characteristics, regardless of the value of constitutive parameter a (Figures 4c and 5c). For the slip law a quiescence follows the rate increase, and the Omori decay constant is most consistent with $p \sim 2$ (equation (4)). The rapid decay in $r(t)/r_0$ predicted by the slip law model is a consequence of faults being able to fail nearly instantaneously even when perturbed relatively early in their cycles (earlier in the cycle than even a Coulomb model would predict; Figure 4b). This leads to a relative abundance of failures at short t and thus a steeper decay rate of $r(t)/r_0$. To understand why this is so, we summarize the slip evolution of an individual fault governed by the slip law. In the initial stages of the loading cycle, no strengthening occurs, and the fault is nearly locked. When a stress step is applied, there is an abrupt strengthening, which damps out the effect of the perturbation, and the fault returns to its nearly locked condition. Thus, for this portion of the cycle the clock advance is nearly indistinguishable from the Coulomb model prediction (Figures 4b and 5b). Once the slip velocity is sufficiently high, a stress step causes the fault to weaken abruptly and to fail almost instantaneously. The weakening is not quite instantaneous as in the Coulomb model and, because it depends on slip velocity and state, can occur earlier in the cycle than the instantaneous failure predicted by the Coulomb model. Mathematically, this strengthening and weakening is governed by how state varies or $d\xi/dt$ and the fact that $d\xi/dt$ depends linearly and logarithmically on $V\xi/d_c$ (equation (3b)). The logarithmic dependence is much slower than linear and causes $d\xi/dt$ to change from ~ 0 or positive (strengthening) to negative (weakening) only when $V\xi/d_c$ becomes sufficiently large (i.e., >1). Early in the cycle, V is increasing but is sufficiently small that $d\xi/dt \sim 0$. An early stress step causes an abrupt velocity increase but only enough that still $V\xi/d_c < 1$, resulting in a positive step in $d\xi/dt$ (i.e., an abrupt strengthening that damps the perturbation). For a later stress step, V is sufficiently large that the resulting abrupt velocity increase makes $V\xi/d_c > 1$ and $d\xi/dt$ very negative (i.e., an abrupt weakening leading to quick failure).

3.2.4. Rate-state, slowness law model seismicity rate change. The slowness law model in which $a = 0.01$, consistent with laboratory estimates, predicts an aftershock sequence duration t_a/t_{cycle} that is longer than most observed. The fact that $t_a = 0$ for the Coulomb model suggests that more Coulomb-like models will have shorter durations. As will be demonstrated in section 4, decreasing a leads to a more Coulomb-like response. *Dieterich* [1994] defined t_a explicitly for the approximate slowness law as

$$t_a = a\sigma_n/(d\tau_b/dt) = a/(kV_b), \tag{6}$$

which also shows that decreasing a (or increasing kV_b) shortens t_a. Thus we decrease a by an order of magnitude and show the resulting predictions of $r(t)/r_0$ in Figure 5. The duration predicted by the slowness law is now closer to the observational constraints.

Although we certainly have not tested all possible models, we find that if all other parameters are appropriate to earthquakes in the Earth, then a better fit to the average characteristics of aftershock sequences requires that a be lower than typical laboratory values of 0.005 to 0.02 [*Dieterich*, 1994]. Alternatively and/or additionally, the stiffness k may be higher

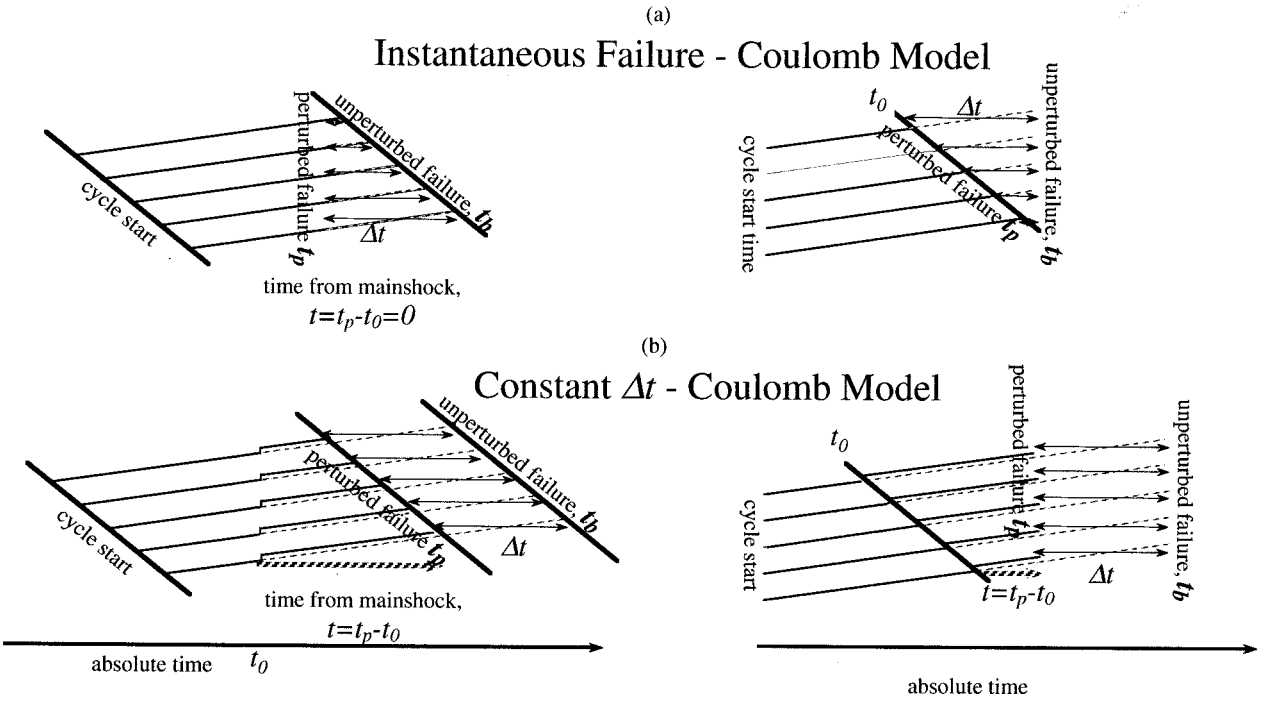

Figure 3. Stress histories predicted for a Coulomb model on the fault populations described in Figure 1, plotted in the same format. Populations on the left correspond to those that might be appropriate to faults affected by a mainshock. The stress is distributed so that when stressed at a constant rate, failure occurs at a constant rate r_0. Populations on the right correspond more appropriately to our approach to calculation of $r(t)$. (a) The effect of a stress step perturbation added to faults that are already stressed to within $\Delta t_{\text{Coulomb}}$ of their unperturbed failure times at t_0. The clock advances cause all the faults to fail instantaneously at t_0 so that $r(t) = dn/dt$ becomes infinite (note the vertical failure line on the left). (b) As in Figure 3a except that the stress step perturbation is added to faults that are farther from failure than $\Delta t_{\text{Coulomb}}$ at t_0. Because Δt is constant, the perturbation does not change the seismicity rate, as indicated by the parallel thick diagonal lines with slopes proportional to $dn/dt = r(t) = r_0$ (left).

than typically thought appropriate for the Earth [*Walsh*, 1971; *Tse and Rice*, 1986; *Sleep*, 1995; *Roy and Marone*, 1996], and σ_n may be less than lithostatic to fit the aftershock seismicity characteristics. *Gross and Kisslinger* [1997] and *Gross and Burgmann* [1998] also reached a similar conclusion using the *Dieterich* [1994] approach to estimate $a\sigma_n$ from aftershocks of the Loma Prieta and Landers, California, earthquakes, respectively. Because they could not estimate these parameters independently, they also considered the possibility that high pore pressures lowered the effective σ_n from lithostatic by about an order of magnitude. *Toda et al.* [1998] studied aftershocks of the Kobe, Japan, earthquake and found $a\sigma_n = 0.35$ MPa, which they interpreted only as implying $\sigma_n = 0.5$ to 2.0 MPa, although they did not comment on how such low values might be achieved. Most recently, *Belardinelli et al.* [1999] applied rate-state theory to model the delay between subevents of the Irpinia, Italy, earthquake and found $a\sigma_n = 0.8$ to 0.9 MPa. They also note that this may imply a low effective normal stress. Our models do not explicitly require specification of σ_n, although we did assume $\sigma_n = 100$ MPa to estimate k from field observations of $k\sigma_n$. We have not explored models with stiffnesses consistent with low normal stresses, so this ambiguity remains a subject for future work. We also have not investigated the effect of varying V_b.

4. Theoretical Comparison of Rate-State and Coulomb Models

We present a simple theoretical analysis that demonstrates how and why the timing of failure predicted by the Coulomb and rate-state models differs and under what conditions the models become nearly identical. Four illustrative examples are shown using the same numerical calculation scheme as for the seismicity rate changes, except that only a single fault is considered and parameters match those measured in the laboratory, where such predictions might be testable.

4.1. Theory

Because the rate-state failure criterion invokes a velocity failure threshold, examining the evolution of velocity is a direct approach to characterizing failure. It is also appropriate for field-based failure studies because slip and slip rate are potentially measurable field quantities. We explore theoretically the evolution of slip and the timing of failure in response to stress history for a rate-state model by deriving equations describing the slip velocity and acceleration. Simple approximate equations for the slip acceleration are derived that are valid for most of the earthquake cycle time. The velocity is described exactly by rearranging the standard frictional rate-state constitutive relation (equation (1)), so that

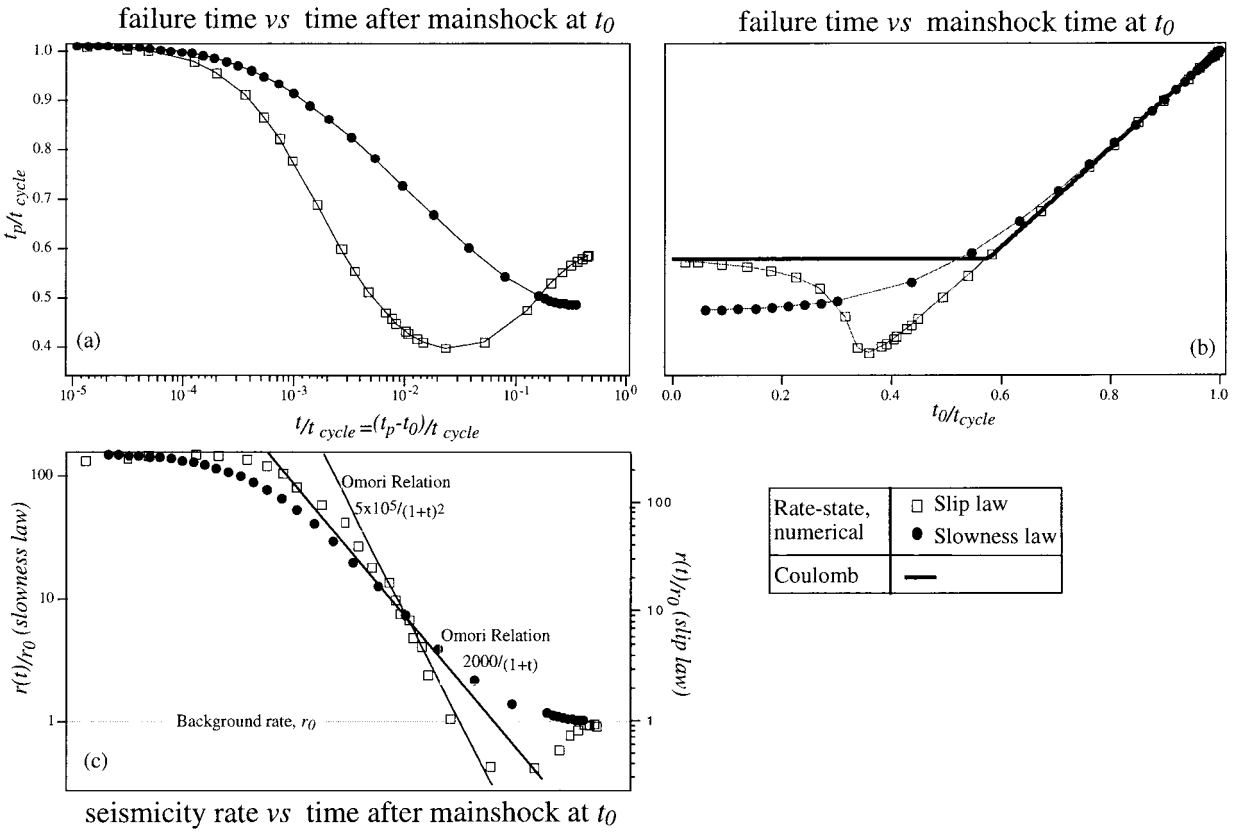

Figure 4. Plots showing seismicity rates and failure times calculated numerically for a rate-state model with constitutive parameter $a = 0.01$ for the slowness law (solid circles) and slip law (open squares) and the corresponding Coulomb model (thick solid lines). All model parameters are listed in Table 1, and all times are normalized by the unperturbed cycle time t_{cycle}. (a) Failure times t_p as a function of the time t from the time of the "mainshock" or equivalently from the perturbing stress step at t_0 (see Figure 1). (b) Failure times t_p as a function of the stress step onset time t_0. (c) The $r(t)/r_0$ calculated numerically according to (5) from the points in Figure 4a. Hypothetical examples of aftershock rates following Omori's law (equation (4)) that fit these decay rates are shown (diagonal lines) with the parameters defining (4) listed; a closer fit at very short times can be obtained by increasing the constant added to t in the denominator, but such large values are not commonly observed.

frictional stress or load is the independent variable. A similar approach was taken in the work of *Sleep* [1995, 1997] and differs from other failure studies in which frictional stress (strength) and the applied shear stress are considered independently, with failure occurring when the applied stress reaches the frictional strength (e.g., as in Coulomb models). Alternatively, in rate-state models the fault slips during the loading cycle so that the fault strength determines the shear stress and one variable simultaneously represents both applied shear stress and frictional strength. A final justification for this approach is the fact that the frictional rate-state constitutive relation is empirically derived, with physical interpretations subsequently ascribed to it. Thus we can interpret it without appealing to the idea of independent frictional strength and loading stress and instead consider it as a description of the evolution of slip velocity.

Equation (1) may be rearranged as a description of the slip velocity variation with stress $\tau(t)$ and $\xi(t)$, written as

$$\begin{aligned} V(t) &= V_c \xi(t)^{-b/a} \exp\left[\tau(t)/(\sigma_n a)\right] \\ V_c &= \exp\left\{-[\mu_0 + a \ln V_0 - b \ln V_0/d_c]/a\right\} \\ &= \exp\left\{-\tau_0/[\sigma_n a]\right\}. \end{aligned} \tag{7}$$

The exponential term of $V(t)$ has the same form as descriptions of thermally activated creep processes [*Sleep*, 1997] or the rate of chemical reactions at crack tips [*Lockner*, 1998]. Thus a^{-1} is a measure of the potency of these processes to change the slip velocity in response to stressing. The preexponential term may represent compaction creep in which compaction slows slip. If the ease with which shearing can occur within a fault zone is represented by a linear viscosity, then compaction creates a greater number of contacts (represented by increasing ξ) and thus increases this viscosity, slowing the slip [*Sleep*, 1995, 1997]. The relative importance of this preexponential term is determined by the amplitude of b relative to a.

A description of how slip evolves includes expressions for slip velocity (equation (7)) and acceleration. We find approximate expressions for acceleration, valid for most of the loading cycle, by writing

$$\begin{aligned} dV/dt &= \partial V/\partial\tau(\partial\tau/\partial t) + \partial V/\partial\xi(\partial\xi/\partial t) \\ d \ln V/dt &= (1/V)dV/dt \\ &= [1/(\sigma_n a)]\partial\tau/\partial t - [b/(a\xi(t))]\partial\xi/\partial t. \end{aligned} \tag{8}$$

The derivation that follows eliminates $\xi(t)$ from (8), resulting in expressions that depend only on $V(t)$, the constant consti-

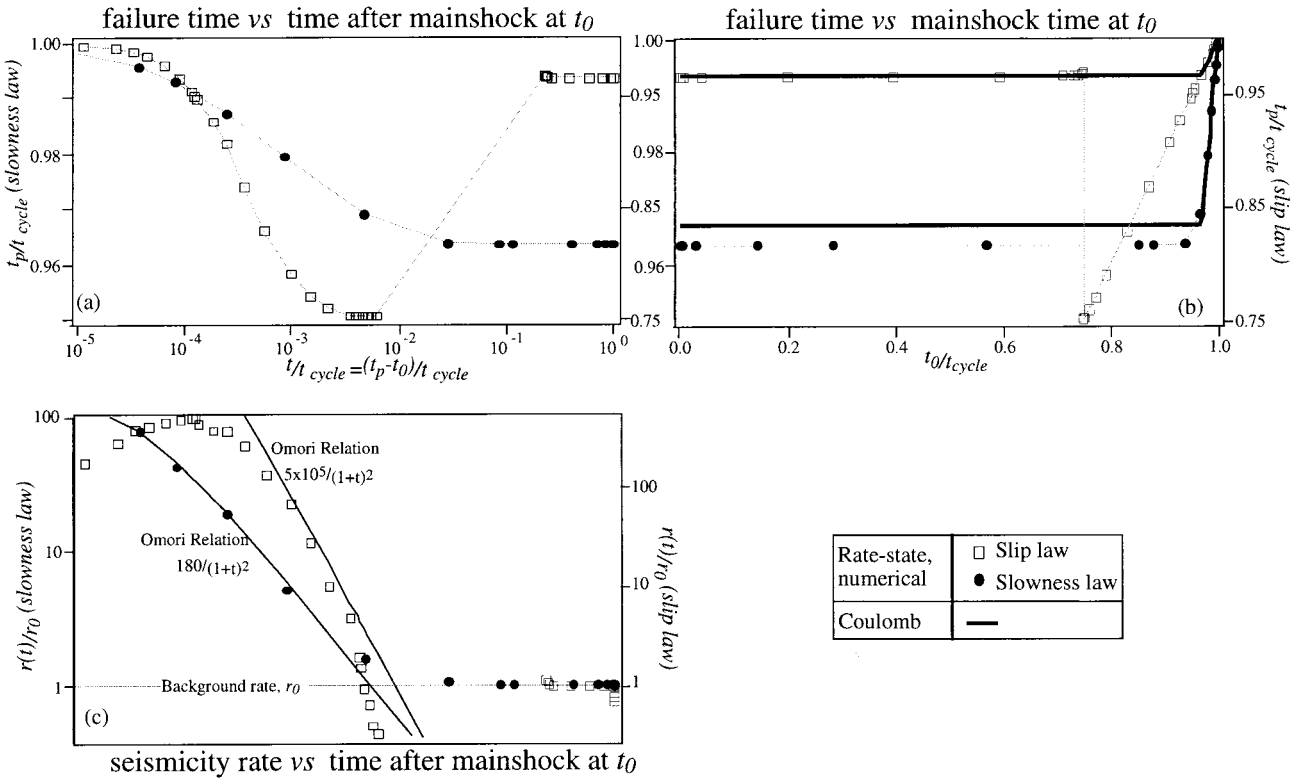

Figure 5. The same as Figure 4, except that the constitutive parameter a is reduced by a factor of 10 or $a = 0.001$, and the load amplitudes are scaled similarly (Table 1). This reduction in a makes the response more Coulomb-like and thus shortens the duration of the aftershock sequence. This intuitively seems reasonable because $t_a = 0$ for the Coulomb model and because sharpening the transition from nearly instantaneous failure to failure independent of t_0 determines the shape of $r(t)/r_0$. See section 4 for additional demonstration of this behavior. Note that this shorter duration may be more consistent with the most commonly observed aftershock sequence characteristics.

tutive parameters, and the stress history. *Dieterich* [1994] derived analytic expressions valid only for the self-accelerating portion of the cycle and the slowness law. We derive approximate expressions that are valid both early and late in the cycle for both the slowness and slip laws.

At the start of the cycle and for most of its duration the fault is slipping negligibly and $V \ll V_b$ [e.g., *Rice and Tse*, 1986], which allows us to find expressions for the derivatives in (8). In the absence of any perturbing stress, (2b) becomes $d\tau(t)/dt \sim \sigma_n k V_b$, and the state evolution laws also may be simplified. When $V\xi/d_c < 1$, we approximate the slowness law (equation (3a)) and state it as $d\xi/dt \sim C$ and $\xi \sim Ct + \xi_{\text{init}}$, in which constant $C \sim 1$. For the slip law, $d\xi/dt \sim 0$ and $\xi \sim \xi_{\text{init}}$ (equation (3b)). In either case, ξ_{init} is a positive constant, and because ξ represents measures of contact connectivity, it is small at the start of a cycle as contacts have just been broken ($\xi \ll d_c/V$ or less than the time required to slip the critical distance). Substitution of these approximations into (8) shows that the slip accelerates according to

$$d \ln V/dt = (1/V)dV/dt = [kV_b - b/(Ct + \xi_{\text{init}})]/a \qquad (9a)$$

for the slowness law or

$$d \ln V/dt = (1/V)dV/dt = [kV_b - bV/d_c \ln (d_c/\xi_{\text{init}}V)]/a \qquad (9b)$$

for the slip law.

When $V\xi/d_c \gg 1$, the system is in its final self-accelerating phase. An expression for the acceleration valid during this phase is obtainable for the slowness law, noting that $d\xi/dt \sim -V\xi/d_c$. Equation (8) becomes

$$d \ln V/dt = (1/V)dV/dt = [kV_b + bV/d_c]/a. \qquad (9c)$$

Although no such approximate solution exists for the slip law, note that when $V\xi/d_c > 1$, then $d\xi/dt < 0$, indicating weakening as for the slowness law. Moreover, the logarithmic term in the slip law grows slowly so that in this phase $d\xi/dt$ is proportional to $-V\xi/d_c$ just as for the slowness law. Thus conclusions we draw from analysis of (9c) are probably valid for the slip law as well.

4.2. Examples

Figures 6–9 illustrate the dependence of Δt on t_0 and the evolution of stress, slip rate, and state over a single earthquake cycle, calculated numerically (see section 2.2). The parameter values (Table 2) were chosen to be similar to those measured in the laboratory [*Blanpied et al.*, 1999]. Figures 6 and 7 illustrate the behavior of "soft" (low k) systems, calculated using the slip law and the slowness law. Figures 8 and 9 show corresponding results for a more "stiff" system. The differences in responses do not simply reflect the different stiffnesses, as the initial conditions also differ so that the cycle times are of similar order. Each figure shows behaviors with and without

step perturbations, each for larger and smaller values of constitutive parameter a.

Equations (9a) and (9b) show explicitly that as a decreases, the fault becomes more Coulomb-like; that is, it remains essentially locked while being stressed. Figures 6–9 illustrate the predictions of these equations. We first discuss conditions under which faults governed by the rate-state laws share this Coulomb characteristic. Equations (9a) and (9b) suggest a simple physical interpretation that for either state evolution law the slip history is determined by a competition between processes that promote and inhibit slip. In other words, the logarithmic change in slip velocity (or $(1/V)dV/dt$) is proportional to the difference between the acceleration due to stressing and deceleration due to strengthening. The acceleration (positive term in (9a) or (9b)) depends linearly on the shear stressing rate $d\tau_b/dt = \sigma_n k V_b$ and the deceleration (negative term in (9a) or (9b)) depends nonlinearly on the strengthening rate. The fact that the change in slip velocity varies at rates inversely proportional to a (see Figures 6c, 7c, 8c, and 9c) leads to the asymptotic behavior of the rate-state model to one that is Coulomb-like when a is small. The initial conditions and magnitude of b are such that the slip initially decelerates (ξ_{init} small and $\xi_{\text{init}} V \ll d_c$; see Table 2) and then begins accelerating. The deceleration is nonlinear and thus much more rapid than the linear acceleration that follows. The inverse dependence of d ln V/dt on a means that smaller a values imply greater initial deceleration to significantly lower initial sliding velocities, and the fault becomes more like one that is locked. Figures 7a and 7c illustrate this most clearly. Physically, this may be understood by noting that when a decreases, the strengthening terms weighted by b effectively become more

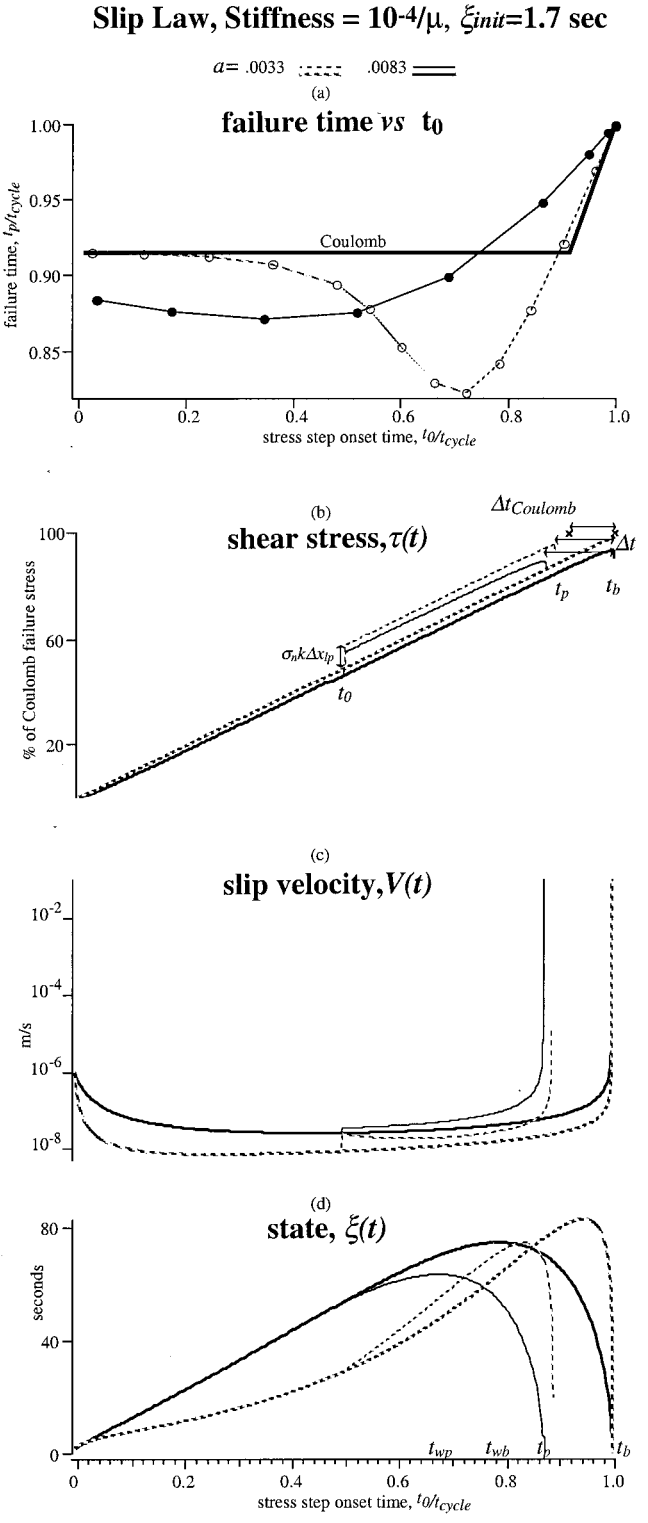

Figure 6. (opposite) Results of numerical calculations for model parameters that correspond to those measured for Westerly granite with initial conditions chosen to produce cycle times comparable to those measured in stick-slip experiments (see Table 2). Two sets of calculations are shown; solid and dashed curves show results for larger and smaller values of a (equation (1)), respectively. All times are normalized by the unperturbed cycle time. A slip law (equation (5b)) governs the state evolution. (a) Failure times as a function of the onset time of a perturbing step function stress. All parameters were kept constant except a in the rate-state calculations. The Coulomb failure time is shown as the thicker straight-line segments; it is constant until failure is immediate. Circles correspond to numerical calculations (connecting curves are for visual aid). (b) Normalized shear stress as a function of the fractional cycle time for some of the calculations used to generate Figure 6a. Stresses are normalized by the shears stress that would accumulate linearly at a constant background rate in the unperturbed cycle time. Thicker and thinner curves show $\tau(t)$ for stressing at a constant background rate only and with a perturbation added halfway through the cycle, respectively. Crosses show where failure would occur for a Coulomb model with the corresponding clock advance indicated by the double arrowhead line. Clock advances for the rate-state models are shown similarly for the two a values. (c) $V(t)$ corresponding to the same set of calculations in Figure 6b. The fact that the change in slip velocity with time varies inversely proportionally to a leads to the asymptotic behavior of the rate-state model to one that is Coulomb-like for the smaller value of a. This is because smaller a values imply greater initial deceleration to significantly lower initial sliding velocities, so the fault becomes more like one that is locked. (d) The $\xi(t)$ corresponding to the same set of calculations in Figure 6b.

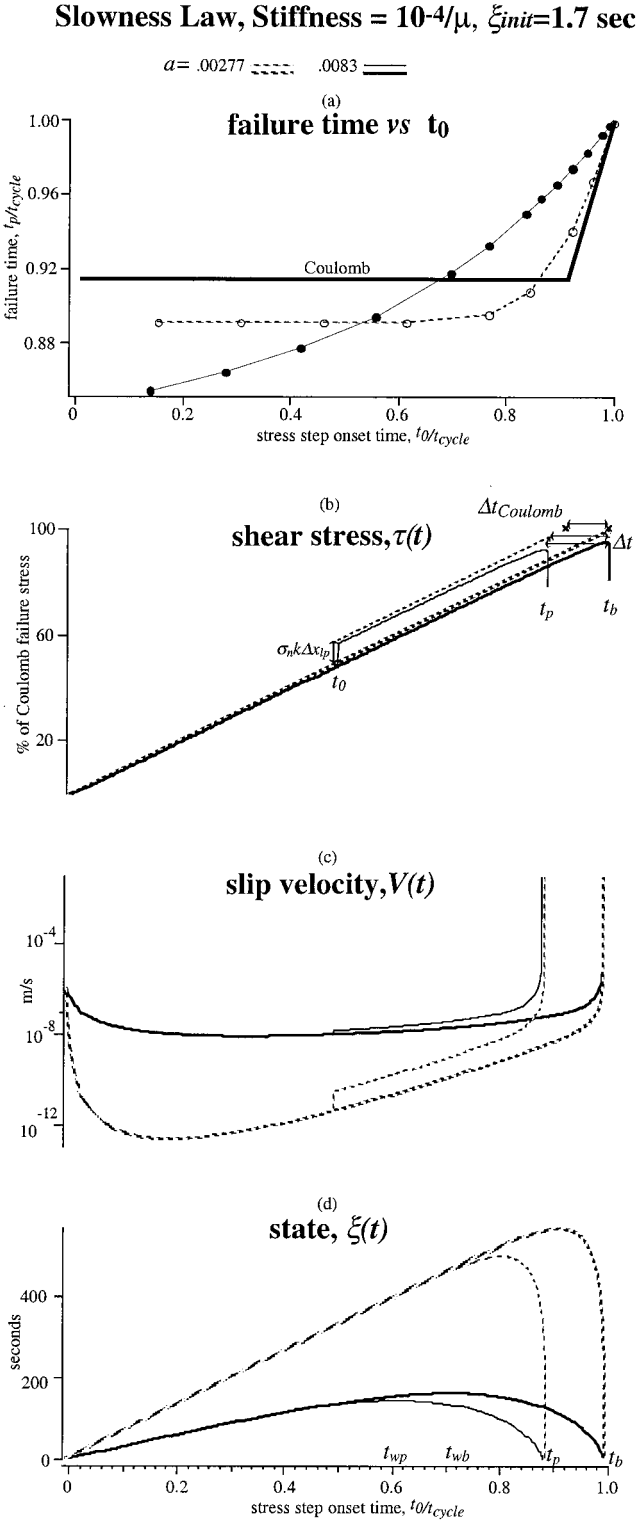

Figure 7. Same as Figure 6, except a slowness law (equation (3a)) governs the state evolution. This example illustrates well how the initial locking up (slowing down) becomes more significant for a smaller value of a. This is because smaller a values imply greater initial deceleration to significantly lower initial sliding velocities so the fault becomes more like one that is locked.

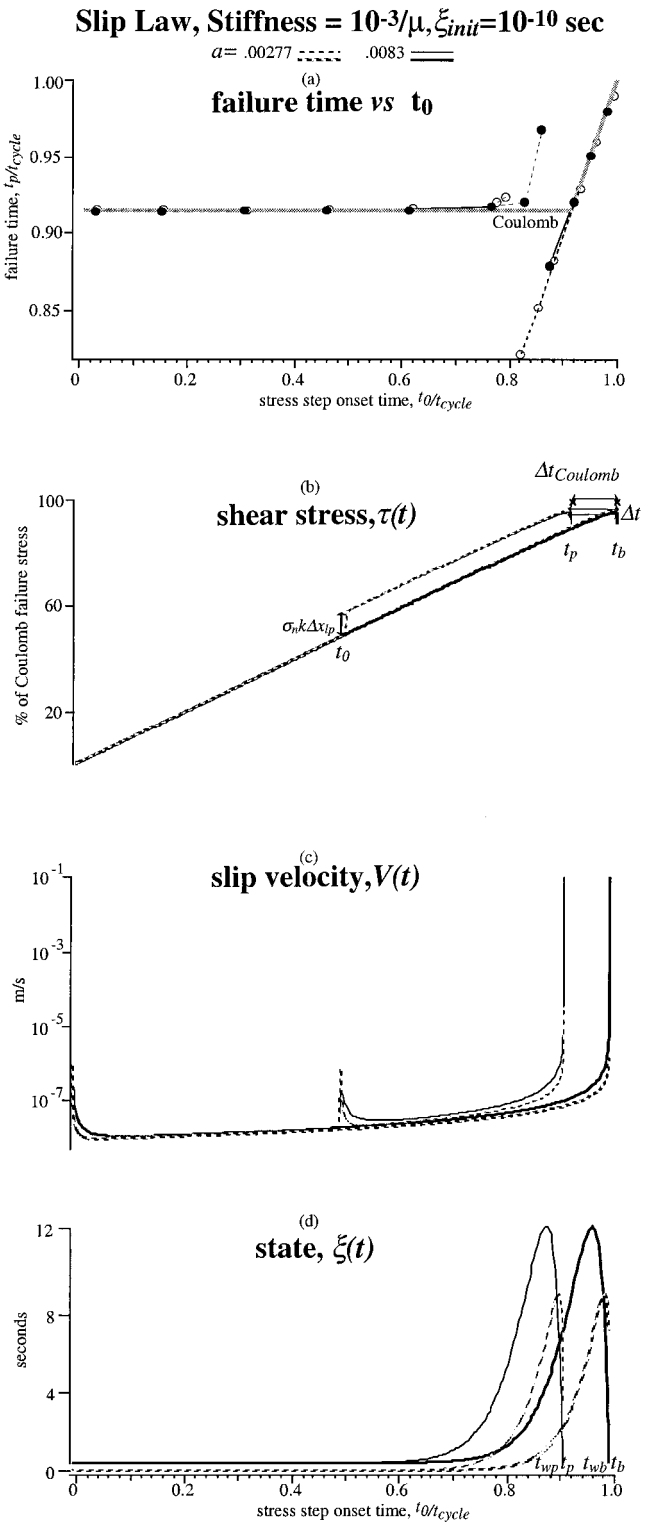

Figure 8. Same as Figure 6, except for a larger stiffness and smaller ξ_{init}. The reduction in ξ_{init} is required to make the cycle times comparable. The greater similarity between the Coulomb and rate-state predictions in Figure 8a, relative to those in Figures 6a and 7a, is a consequence both of the increased stiffness and different initial conditions.

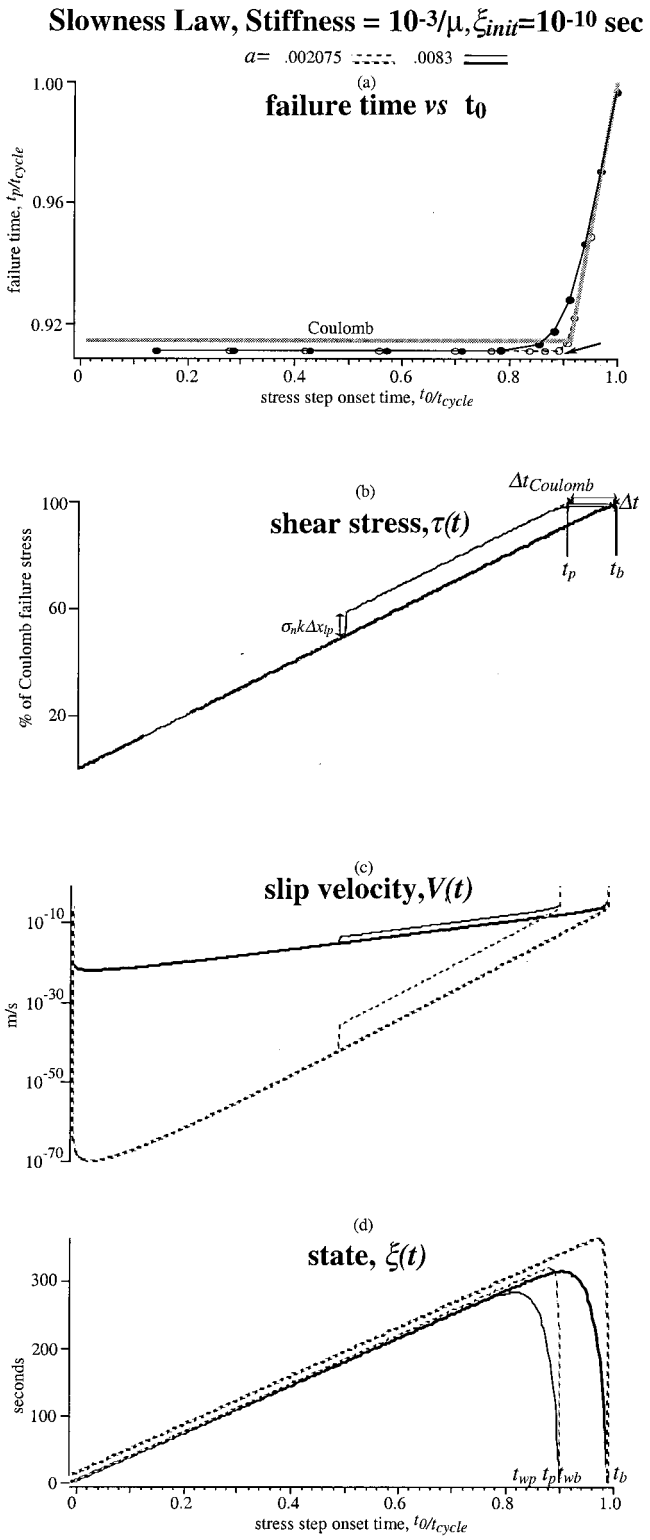

Figure 9. Same as Figure 7, except for a larger stiffness and smaller ξ_{init}. The reduction in ξ_{init} is required to make the cycle times comparable. This example illustrates well how the initial locking up (slowing down) becomes more significant for a smaller value of a. The greater similarity between the Coulomb and rate-state predictions in Figure 9a, relative to those in Figures 6a and 7a, is a consequence both of increased stiffness and different initial conditions.

important. Thus the "locking up" of the fault may be interpreted as a consequence of rapid initial healing of fault contacts, which becomes more pronounced as a is decreased relative to b.

Another characteristic of Coulomb models is that failure occurs instantaneously. The rate-state response more closely approximates this as a becomes smaller relative to b because the condition $V\xi/d_c \ll 1$ becomes true for a longer fraction of the cycle, so the rapid self-acceleration to failure happens over a shorter time. Moreover, once the self-accelerating state is reached, smaller a values imply more rapid acceleration to failure. Equation (9c) also describes this for the slowness law. Note that $d \ln V/dt$ is always positive and is inversely proportional to a. Equation (9c) implies more rapid acceleration at the end of the cycle, because of its additional dependence on V, than does equation (9a), which applies to the rest of the cycle (e.g., see Figures 2a and 2c). (The behavior described by (9c) will be true even when $V \sim V_b$ and $d\mu/dt \sim 0$ or when $V \gg V_b$ and $d\tau/dt \sim -\sigma_n kV$. In these cases, $d \ln V/dt = bV/d_c a$ or $d \ln V/dt = V/a[-k + b/d_c]$ respectively. The latter derivative is always positive because the rate-state model requires that $k < (b - a)/d_c$ for instability to be possible [*Ruina*, 1983].)

Finally, Δt predicted by the Coulomb model is independent of stressing history or, equivalently, of t_0. During the early portion of the cycle (i.e., when $V\xi/d_c \ll 1$), clock advances are more Coulomb-like, being less dependent on when stress steps are applied than later in the cycle. This early portion becomes a greater fraction of the cycle as a is decreased. The derivations below demonstrate this behavior (Figures 6a and 6c, 7a, and 7c). Combining (7) with (2) and ignoring the change in ξ at t_0 yields an expression for the velocity change caused by a stress step (see Appendix B). For systems governed by either the slowness law or the slip law this velocity change is

$$\Delta \ln V \sim k\Delta x_{lp}/a, \tag{10}$$

which is independent of the time the stress step is applied, t_0. If perturbed after the initial deceleration and before the final self-accelerating phase, then the log velocity changes at a rate proportional only to the background stressing rate, $d\tau_b/dt = \sigma_n k V_b$. Mathematically, from (9a) or (9b) this may be stated as

$$d \ln V/dt = kV_b/a. \tag{11}$$

The clock advance is the time required to change the velocity when stressed at constant rate V_b by an amount equal to that caused by a stress step or $\Delta t \sim \Delta \ln V/[d \ln V/dt]$. Thus by comparing (10) and (11) we find that the clock advance is

$$\Delta t \sim \Delta x_{lp}/V_b. \tag{12}$$

This is simply the Coulomb clock advance $\Delta t_{\text{Coulomb}}$.

Figures 6, 7, and 9 show that although both Coulomb and

Table 2a. Fixed Parameters for Rate-State Models in Figures 6–9

Parameter	Value
b	0.0127
μ_0	0.75
V_0, μ/s	1
d_c, μ	3
V_{init}, μ/s	1

Initial values V_{init} and ξ_{init} and constants μ_0 and V_0 were chosen so that all numerical experiments resulted in comparable cycle times.

Table 2b. Varied Parameters for Rate-State Models in Figures 6–9

	State Evolution Law	a	k, μ^{-1}	ξ_{init}, s	Δx_{lp}, μ	Cycle Time, s
Figure 6	slip	0.0083	10^{-4}	1.662 (1%)	24.748	289.281
		0.0033	10^{-4}	1.662 (1%)	35.525	415.242
Figure 7	slowness	0.0083	10^{-4}	1.662 (1%)	30.636	358.667
		0.00277	10^{-4}	1.662 (1%)	55.683	650.871
Figure 8	slip	0.0083	10^{-3}	1.653×10^{-10} (40%)	27.903	326.151
		0.00277	10^{-3}	1.653×10^{-10} (40%)	27.582	322.408
Figure 9	slowness	0.0083	10^{-3}	1.653×10^{-10} (40%)	30.000	350.667
		0.002075	10^{-3}	1.653×10^{-10} (40%)	30.648	358.244

Percentages specified next to ξ_{init} values indicate the corresponding initial value of μ relative to μ_0. The values of stiffness k, larger value of a, b, d_c, load point displacement Δx_{lp}, and cycle times are similar to those measured in laboratory experiments [*Blanpied et al*., 1999]. Initial values V_{init} and ξ_{init} and constants μ_0 and V_0 were chosen so that all numerical experiments resulted in comparable cycle times.

rate-state model predictions may be independent of when the perturbing stress is applied, the magnitudes of the clock advances may differ. We show how this arises and find that the rate-state clock advance approaches the Coulomb prediction (i.e., equation (12)) when b becomes small relative to the background-stressing rate, $\sigma_n k V_b$. Recalling that t_p and t_b represent the failure times with and without a stress step perturbation (see Figures 6b, 6d, 7b, 7d, 8b, 8d, 9b, and 9d), we obtain an expression for clock advance, $\Delta t = t_b - t_p$. This is done by equating $V(t_p) = V(t_b)$ in accord with a velocity failure criterion, neglecting precursory slip (Appendix C), and noting that the stress prior to t_0 is the same with and without the stress step. From (7) we obtain the relation

$$\Delta t = \Delta x_{lp}/V_b + b/kV_b \ln [\xi_b(t_b)/\xi_p(t_p)]$$
$$= \Delta t_{\text{Coulomb}} + b/kV_b \ln [\xi_b(t_b)/\xi_p(t_p)]. \quad (13)$$

In most cases, the rate-state clock advance exceeds that predicted by the Coulomb model. This is because the term determining the difference, $\xi_b(t_b)/\xi_p(t_p)$, exceeds or equals one for perturbations applied during most of the cycle (see Appendix D). The slip law model shown in Figure 8 is the exception to this; the reason for its behavior was discussed in section 3.

Equation (13) highlights a fundamental difference between the failure criteria of the rate-state and Coulomb models and shows that for most of the loading cycle the rate-state clock advance exceeds $\Delta t_{\text{Coulomb}}$. In the latter, failure occurs when the loading stress reaches some threshold failure stress, but there is no stress threshold in the rate-state model. Equation (13) implies that one can think of a rate-state model as a modified Coulomb failure model in which the failure stress threshold is lowered (Figures 6b, 7b, and 9b). This effective lowering of the failure threshold and thus earlier failure correspond to $\xi_b(t_b)/\xi_p(t_p) > 1$ in (13). An effective lowering of the failure stress threshold by the same amount with and without the step perturbation is what happens for the stiff system governed by the slip law (Figure 8b) during most of the cycle and corresponds to $\xi_b(t_b)/\xi_p(t_p) = 1$ in (13).

Thus far we have explored the dependence of the rate-state model on the constitutive parameters a and b. As (9) and Figures 6–9 indicate, deviation from Coulomb-like behavior also depends on the stiffness and loading velocity (or stressing rate $d\tau_b/dt$) and the initial conditions. The greater similarity between the Coulomb and rate-state predictions in Figures 8a and 9a relative to those in Figures 6a and 7a is a consequence both of the increased stiffness and different initial conditions. The stiffer model parameters actually correspond to those measured in the laboratory [*Blanpied et al*., 1999] with ξ_{init}, for which we have no direct measurement, adjusted to match the observed cycle time. When exploring the effect of k by reducing it (Figures 6–7), we adjusted ξ_{init} to keep the cycle time of the same order. As (9a) and (9b) indicate, ξ_{init} may have profound effect on the initial deceleration and thus the evolution of slip. Further exploration of the dependence on these other parameters awaits further work.

5. Conclusions

We examine theoretically the predictions of the timing of earthquake failure for both Coulomb failure stress and rate-state frictional models. A Coulomb model requires that a fault remain locked during stressing, that failure occur instantaneously and that changes in failure time (clock advances, Δt) associated with a static stress step are independent of when it is applied. Clock advances predicted by rate-state models asymptotically become equivalent to Coulomb predictions under a variety of conditions. If the rate-state constitutive parameter a is decreased relative to b, the fault motion becomes more nearly stationary or locked, acceleration to instability approaches instantaneous failure, and Δt associated with static stress becomes independent when it is applied. If a is decreased, the strengthening terms weighted by b effectively become more significant. Thus the locking up of the fault may be interpreted as a consequence of rapid initial healing of fault contacts, which becomes more pronounced as a is made small relative to b. Our analysis shows that even when Δt predicted by rate-state has these same characteristics, its magnitude may differ by some constant from the Coulomb model prediction. This constant difference depends on the constitutive parameter b, which weights the terms describing how the connectivity of fault contacts evolves with time. One way to understand this difference is to consider a rate-state model as a modified Coulomb failure model in which the failure stress threshold is lowered, thereby increasing the clock advance.

We also examine changes in seismicity rates $r(t)/r_0$ due to coseismic static stress increases which, in the case of aftershocks, cannot be explained by a Coulomb failure model. We find that rate-state model faults must be Coulomb-like (i.e., have the characteristics of a Coulomb model listed above) to match an Omori law decay in seismicity rate (i.e., a value of $p \sim 1$), have an aftershock duration that is considerably less than a few percent of the cycle time, and to return directly to the background rate from an increase. Also, the constitutive parameter a may be lower than values typically estimated in the laboratory. Alternatively or additionally, the stiffness may

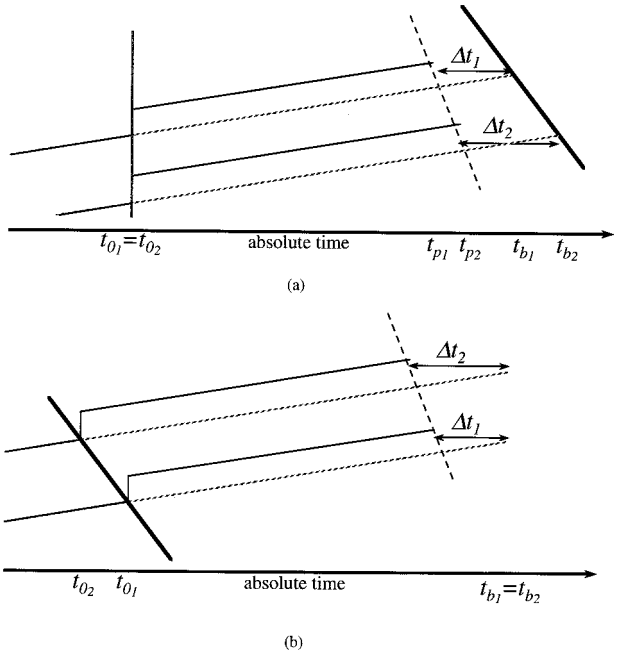

Figure A1. Expanded version of Figure 1 for just two faults. Note that $t_{b2} - t_{b1}$ in Figure A1a equals $t_{01} - t_{02}$ in Figure A1b. See text for explanation.

be high and normal stress lower than lithostatic. Our analysis shows explicitly that the faults that participate in an aftershock sequence are only those that are on the brink of failure at the time of the mainshock (i.e., would have failed within less than a few percent of the total cycle time in the absence of the mainshock). Finally, although not exhaustive, our modeling suggests that the slip evolution law is inconsistent with characteristics of aftershock seismicity.

Appendix A

We define the seismicity rate as $r(t) = dn/dt$, in which n indicates the number of earthquakes that fail at time t after a perturbation is applied at t_0, and $t = t_p - t_0$, in which t_p is the perturbed failure time. Assume background seismicity is due to failure of a collection of faults, each at a different fraction of its unperturbed cycle duration. These fractions are initially distributed evenly from zero to one such that the seismicity rate resulting from stressing at a constant rate is a constant r_0 (Figure 1a). We derive general equations for $r(t)$ by considering just two faults (Figure A1a). The seismicity rate estimated in the absence of any perturbation is simply the difference in their unperturbed failure times t_{b_1} and t_{b_2} or

$$1/r_0 = [t_{b_2} - t_{b_1}]/\Delta n \tag{A1}$$

($\Delta n = 1$ in Figure A1). A perturbation advances the failure times by Δt_i ($i = 1, 2$), resulting in a new seismicity rate r or

$$1/r = [(t_{b_2} - \Delta t_2) - (t_{b_1} - \Delta t_1)]/\Delta n. \tag{A2a}$$

Rearranging this yields

$$\begin{aligned} 1/r &= [(t_{b_2} - t_{b_1}) - (\Delta t_2 - \Delta t_1)]/\Delta n] \\ &= 1/r_0 - (\Delta t_2 - \Delta t_1)/\Delta n \\ &= 1/r_0 - (\Delta \Delta t/\Delta t_b)(\Delta t_b/\Delta n) \\ &= 1/r_0[1 - (\Delta \Delta t/\Delta t_b)]. \end{aligned} \tag{A2b}$$

Previous studies of single fault systems have shown that clock advance Δt for a single fault may depend on t_0 [*Gomberg et al*., 1997, 1998]. This dependence may be computed numerically or analytically in special circumstances, and such computations may be employed to calculate $r(t)$ by considering an equivalent distribution of faults to the one described above. In this alternative distribution, all faults are advanced by the same amount in their cycles and then perturbed at different t_0, and all unperturbed failure times are equal (Figure 1b). Noting that Δt_b in (A2b) is equivalent to $-\Delta t_0$ in this alternative distribution (Figure A1b) results in

$$r(t) = r_0/[1 + \Delta \Delta t/\Delta t_0], \tag{A3a}$$

with differential form

$$r(t) = r_0/[1 + d\Delta t/dt_0]. \tag{A3b}$$

This can be rewritten in terms of t_p as

$$r(t) = r_0/[1 - dt_p/dt_0] \tag{A3c}$$

because $\Delta t = t_b - t_p$, and t_b is constant in this population (Figure 1b). These equations are convenient, allowing $r(t)$ to be calculated numerically; t_p is computed for a series of calculations, each time varying t_0, and associated with the time $t = t_p - t_0$. Equation (A3) can also be recast in terms of t directly, noting that $dt_0/dt = dt_p/dt - 1$ and $dt_p/dt_0 = (dt_p/dt)/(dt_0/dt)$, so that by substitution

$$r(t) = r_0[1 - dt_p/dt]. \tag{A4}$$

Appendix B

The stress change due to a step perturbation is $\Delta\tau = \sigma_n k \Delta x_{lp}$ (from (2), since $\Delta x/\Delta x_{lp} \sim 0$ for most of the cycle). The effect of $\Delta\tau$ on slip velocity is easily seen by substituting $\Delta\tau$ into (7) and letting t_0^+ and t_0^- represent the instants before and after t_0, respectively. The ratio of the velocities at these times is

$$V(t_0^+)/V(t_0^-) = [\xi(t^+)/\xi(t^-)]^{-b/a} \exp[k\Delta x_{lp}/a]$$

or

$$\Delta \ln V = -b/a \ln[\xi(t^+)/\xi(t^-)] + k\Delta x_{lp}/a. \tag{B1}$$

In many cases the term $\ln[\xi(t^+)/\xi(t^-)]$ may be neglected (see Figures 7d, 8d, and 9d for small a calculations). This is true for both the slowness and slip laws early in the cycle when $V\xi/d_c \sim 0$ so that $d\xi/dt \sim 1$ for the slowness law and $d\xi/dt \sim 0$ for the slip law. Thus early in the cycle the rate of change of ξ becomes constant, and the instantaneous change in ξ from t_0^- to t_0^+ becomes negligible.

Appendix C

An expression relating the Coulomb and rate-state clock advances (i.e. equation (13)) is derived by noting that the stresses just prior to failure with and without the perturbation equals $\sigma_n k[V_b t_p + \Delta x_{lp} - \Delta x_p]$ and $\sigma_n k[V_b t_b - \Delta x_b]$, respectively. Δx_b and Δx_p denote the precursory slip accumulated prior to failure in both cases, and we assume either that $\Delta x_b \sim \Delta x_p$ and/or that the precursory slip is negligible (i.e., $V_b t_p > \Delta x_p$ and $V_b t_b > \Delta x_b$). Both numerical and laboratory models [*Blanpied et al*., 1999] show the latter to be true. *Gomberg et al*. [1998] show that for the slowness law, $\Delta x_b = \Delta x_p$ when the velocity at failure is infinite, suggesting that $\Delta x_b \sim \Delta x_p$ as long as the failure velocity is some high value.

Appendix D

We demonstrate that $\xi_b(t_b)/\xi_p(t_p) > 1$ by first defining the time that weakening begins as t_w when $V(t_w)\xi(t_w)/d_c = 1$ so $d\xi(t_w)/dt = 0$. Failure occurs after t_w and when some high velocity V_f is reached. As discussed in Appendix B, early in the cycle the only effect of the perturbation is to increment $\ln V$. This advances the time weakening commences by an essentially constant amount, dependent only on the magnitude of $\Delta \ln V$. Also, because a perturbation causes an instantaneous increase in velocity (equation (10)), weakening begins earlier and at a lower value of ξ than in the unperturbed case; that is, $\xi_b(t_{wb}) > \xi_p(t_{wp})$, in which t_{wb} and t_{wp} correspond to t_w for the unperturbed and perturbed cases, respectively (see Figures 6d, 7d, and 9d). Suppose failure occurs immediately after weakening begins such that $t_b \sim t_{wb}$ and $t_p \sim t_{wp}$. Thus $\xi_b(t_b) > \xi_p(t_p)$ must be true in general for this special case to satisfy the requirement that $\xi_b(t_{wb}) > \xi_p(t_{wp})$. The same logic explains why the rate-state and Coulomb clock advances are nearly identical for the system governed by the slip evolution law in Figure 8. In this case there is no strengthening (and thus no weakening) through most of the cycle so the effect of a perturbation occurring early in the cycle is to advance the time at which ξ begins to evolve at all (i.e., when $d\xi/dt$ becomes nonzero) by an amount dependent only on the magnitude of $\Delta \ln V$. Thus the perturbed path of $\xi(t)$ to failure will simply be an advanced version of that without a perturbation so that $\xi_b(t_{wb}) = \xi_p(t_{wp})$, $\xi_b(t_b) = \xi_p(t_p)$ and $\Delta t \sim \Delta t_{\text{Coulomb}}$.

Acknowledgments. We thank Massimo Cocco, Susanna Gross, Paul Bodin, Mousumi Roy, and Tom Parsons for their very thoughtful reviews and suggested revisions. We also thank Jim Dieterich for participating in informative discussions. CERI contribution 395.

References

Beeler, N. M., T. E. Tullis, and J. D. Weeks, The roles of time and displacement in the evolution effect in rock friction, *Geophys. Res. Lett*., *21*, 1987–1990, 1994.

Belardinelli, M. E., M. Cocco, O. Coutant, and F. Cotton, Redistribution of dynamic stress during coseismic ruptures: Evidence for fault interaction and earthquake triggering, *J. Geophys. Res*., *104*, 14,925–14,945, 1999.

Blanpied, M. L., J. Gomberg, N. M. Beeler, J. H. Dieterich, B. D. Kilgore, and P. Bodin, Effects of stress history on earthquake timing, *Seismol. Res. Lett*., *70*, 234, 1999.

Dieterich, J. H., Modeling of rock friction, 1, Experimental results and constitutive equations, *J. Geophys. Res*., *84*, 2161–2168, 1979.

Dieterich, J. H., Constitutive properties of faults with simulated gouge, in *Mechanical Behavior of Crustal Rocks: The Handin Volume*, *Geophys. Monogr. Ser*., vol. 24, edited by N. L. Carter et al., pp. 103–120, AGU, Washington, D. C., 1981.

Dieterich, J. H., A model for the nucleation of earthquake slip, in *Earthquake Source Mechanics*, *Geophys. Monogr. Ser*., vol. 37, edited by S. Das, J. Boatwright, and C. Scholz, pp. 36–49, AGU, Washington, D. C., 1986.

Dieterich, J. H., Earthquake nucleation on faults with rate- and state-dependent strength, *Tectonophysics*, *211*, 115–134, 1992.

Dieterich, J., A constitutive law for rate of earthquake production and its application to earthquake clustering, *J. Geophys. Res*., *99*, 2601–2618, 1994.

Gomberg, J., M. L. Blanpied, N. M. Beeler, and P. Bodin, Transient triggering of near and distant earthquakes, *Bull. Seismol. Soc. Am*., *87*, 294–309, 1997.

Gomberg, J., N. M. Beeler, M. L. Blanpied, and P. Bodin, Earthquake triggering by transient and static deformations, *J. Geophys. Res*., *103*, 24,411–24,426, 1998.

Gross, S., and R. Burgmann, Rate and state of background stress estimated from the aftershocks of the 1989 Loma Prieta, California, earthquake, *J. Geophys. Res*., *103*, 4915–4928, 1998.

Gross, S., and C. Kisslinger, Estimating tectonic stress rate and state with Landers aftershocks, *J. Geophys. Res*., *102*, 7603–7612, 1997.

Hardebeck, J. L., J. J. Nazareth, and E. Hauksson, The static stress change triggering model: Constraints from two southern California aftershock sequences, *J. Geophys. Res*., *103*, 24,427–24,438, 1998.

Harris, R., Introduction to special section: Stress triggers, stress shadows, and implications for seismic hazard, *J. Geophys. Res*., *103*, 24,347–24,358, 1998.

Harris, R., and R. W. Simpson, Changes in static stress on southern California faults after the 1992 Landers earthquake, *Nature*, *360*, 313–318, 1992.

Harris, R., and R. W. Simpson, Suppression of large earthquakes by stress shadows: A comparison of Coulomb and rate-and-state failure, *J. Geophys. Res*., *103*, 24,439–24,451, 1998.

King, G. C. P., R. S. Stein, and J. Lin, Static stress changes and the triggering of earthquakes, *Bull. Seismol. Soc. Am*., *84*, 935–953, 1994.

Kisslinger, C., and A. Hasegawa, Seismotectonics of intermediate-depth earthquakes from properties of aftershock sequences, *Tectonophysics*, *197*, 27–40, 1991.

Kisslinger, C., and L. M. Jones, Properties of aftershock sequences in southern California, *J. Geophys. Res*., *96*, 11,947–11,958, 1991.

Lockner, D. A., A generalized law for brittle deformation of Westerly granite, *J. Geophys. Res., 103*, 5107–5123, 1998.

Nakatani, M., A new mechanism of slip weakening and strength recovery of friction associated with the mechanical consolidation of gouge, *J. Geophys. Res*., *103*, 27,239–27,256, 1998.

Nalbant, S. S., A. Hubert, and G. C. P. King, Stress coupling between earthquakes in northwest Turkey and the north Aegean Sea, *J. Geophys. Res*., *103*, 24,469–24,486, 1998.

Nostro, C., R. S. Stein, M. Cocco, M. E. Belardinelli, and W. Marzocchi, Two-way coupling between Vesuvius eruptions and southern Apennine earthquakes, Italy, by elastic stress transfer, *J. Geophys. Res*., *103*, 24,487–24,504, 1998.

Rice, J. R., and S. T. Tse, Dynamic motion of a single degree of freedom system following a rate and state dependent friction law, *J. Geophys. Res*., *91*, 521–530, 1986.

Roy, M., and C. Marone, Earthquake nucleation on model faults with rate- and state-dependent friction: Effects of inertia, *J. Geophys. Res*., *101*, 13,919–13,932, 1996.

Ruina, A., Slip instability and state variable friction laws, *J. Geophys. Res*., *88*, 10,359–10,370, 1983.

Sleep, N. H., Ductile creep, compaction, and rate and state dependent friction within major fault zones, *J. Geophys. Res*., *100*, 13,065–13,080, 1995.

Sleep, N. H., Application of a unified rate and state friction theory to the mechanics of fault zones with strain localization, *J. Geophys. Res*., *102*, 2875–2895, 1997.

Toda, S., R. S. Stein, P. A. Reasenberg, J. Dieterich, and A. Yoshida, Stress transferred by the 1995 $M_w = 6.9$ Kobe, Japan, shock: Effect on aftershocks and future earthquake probabilities, *J. Geophys. Res*., *103*, 24,543–24,566, 1998.

Tse, S. T., and J. R. Rice, Crustal earthquake instability in relation to the depth variation of frictional slip properties, *J. Geophys. Res*., *91*, 9452–9472, 1986.

Utsu, T., Y. Ogata, and R. S. Matsu'ura, The centenary of the Omori formula for a decay law of aftershock activity, *J. Phys. Earth*, *43*, 1–33, 1995.

Walsh, J. B., Stiffness in faulting and in friction experiments, *J. Geophys. Res*., *76*, 8597–8598, 1971.

Wells, D. L., and K. J. Coppersmith, New empirical relationships among magnitude, rupture length, rupture area, and surface displacement, *Bull. Seismol. Soc. Am*., *84*, 974–1001, 1994.

N. Beeler and M. Blanpied, U.S. Geological Survey, MS 977, 345 Middlefield Road, Menlo Park, CA 92045. (nbeeler@isdmnl.wr.usgs.gov; mblanpied@isdmnl.wr.usgs.gov)

J. Gomberg, U.S. Geological Survey, Center for Earthquake Research and Information, University of Memphis, Memphis, TN 38152. (gomberg@usgs.gov)

(Received June 2, 1999; revised November 1, 1999;
accepted December 6, 1999.)